CHAPTER VI

SPATIOTEMPORAL DYNAMICS OF THE 1-D KURAMOTO-SIVASHINSKY EQUATION

In this chapter, we will discuss the spatiotemporal dynamics of the KSe from a periodic orbit theory point of view. In sect. 6.1, after introducing the bifurcation sequence leading to the chaotic solution, we emphasized the dominant role of the coherent structures in the system dynamics and present their sigmificance from a dynamical systems point of view. In sect. 6.2, numerical implementation of the previous discussions is done on the KSe for $L = 38.5\,, \nu = 1$ with periodic boundary conditions. Finally, we summarize the chapter and suggest possible directions for further investigation.

6.1 Review

6.1.1 Bifurcation sequence

One fundamental problem in the dynamical systems approach to turbulence is that: are transitions to chaos true routes to turbulence [48]? This is not obvious since usual dynamical systems have only a few degrees of freedom with no spatial features, while systems described by a PDE have infinitely many degrees of freedom with possibly intricate spatial structures. The KSe provides the simplest example of a nonlinear PDE that exhibits extremely rich dynamical behavior [134] and that can be tackled within the framework of dynamical system theory.

For small system size L, the dynamics and bifurcation sequence are thoroughly investigated both numerically and analytically [133, 146, 6, 125, 140]. When $L < 2\pi\sqrt{\nu}$, as proven in Chapter 5 the origin is the global attractor, with no interesting spatial structure. With L passing $2\pi\sqrt{\nu}$, a supercritical bifurcation generates two stationary attractors with one spatial hump, called unimodal solutions. Due to the inversion invariance in the antisymmetric solution space, these two solutions are half-period translates of each other. At $L = 4\pi\sqrt{\nu}$, new stationary points emerge from the origin with two spatial hump, called bimodal solutions. Later on stable equilibria with n humps are observed with energy concentrating on the nth Fourier modes. A class of such steady attractive solutions are analyzed by Frisch *et. al* [92] and called cellular solution as they exhibit the so-called viscoelastic behavior under long-wave perturbations. One of the two bimodal solutions undergoes a pitchfork bifurcation to a pair of bi-tri pairs at $L \approx 4.7\pi\sqrt{\nu}$, and consequently a Hopf bifurcation to a symmetric limit cycle, at $L \approx 5.3\pi\sqrt{\nu}$, see figure 21. From then on, the bifurcation becomes very complicated. Cycles of various periods, homoclinic and heteroclinic orbits are generated through global and local bifurcations [140]. The SIS are generated via period-doubling cascade and Shilnikov mechanism as well, and they are repellers at emergence. The first

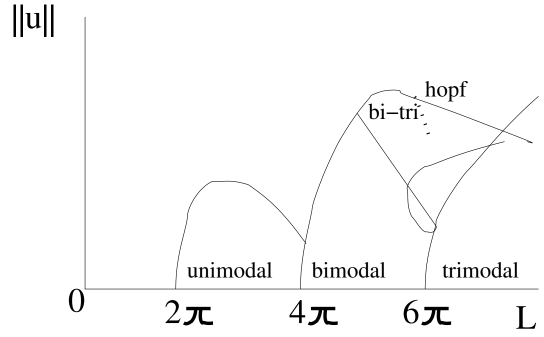

Figure 21: A sketch of the bifurcation diagram of the KSe in the antisymmetric solution space with periodic boundary conditions. The system size L is the bifurcation parameter.

chaotic behavior appear as the competition between two and three hump states. Later on, the regular behavior and the chaotic dynamics alternate. When L is big enough, only chaotic motion is observed numerically. On many parts in the parameter space, there are several attractors coexisting in the phase space. In the full solution space, greater variety of solutions like traveling waves, qusiperiodic solutions appears during the transition to chaos. Chaos mounts on the stage with the two-cellular and three-cellular states competing with each other. Armbruster *et. al* showed that four complex modes are enough to produce all the basic features of the system for a considerably large range of system sizes [6]. But for the full spatiotemporal chaos, we need more modes.

6.1.2 Spatiotemporal chaos and recurrence patterns

J. Hyman and B. Nicolaenko [134] went on to explore dynamics on larger intervals and found that regular and chaotic regions appear alternatively. Intermittency and metastable states are observed for various parameter ranges. For the system size sufficiently large, strange equilibria appear which contain broad spectra of Fourier modes. These equilibrium points bring spatial complexity to the solution and are believed to play an important role in the formation of eventual large-scale spatiotemporal chaos. These points correspond to periodic solutions on the chaotic sets of the ODE for steady solutions of the KSe and were identified by Michelson [178]. Locally coherent structures are frequently observed even in the fully spatiotemporal chaotic regime. The aforementioned cellular structures are the most commonly encountered ones. They are a well-defined entity, moving only slightly chaotically, interacting weakly with each other except at some discrete space-time points where they are annihilated or created, leaving almost constant local cell densities, see figure 22. We can take a portion of the profile of $u(x,t)$ and after small modification of the boundary parts extend it periodically to the whole real axis to get a new profile. For a considerable amount of time, the evolution of these two profiles agrees fairly well, especially in the central part [59, 125]. These observations show that the full chaotic system consists of almost constant number of spatially localized cells or subsystems. They look rather similar and have few internal degrees of freedom which are controllable. They communicate with each other weakly and mainly through their boundaries.

From a dynamical system point of view, the coherent structures with short periods live and are stable in some invariant subspaces of the full phase space. In the spatiotermporal

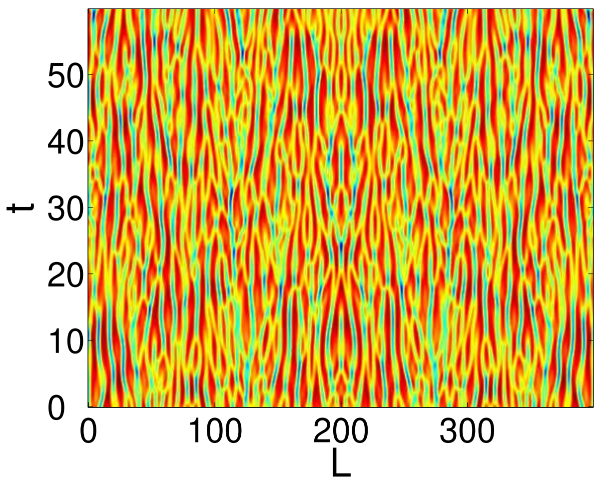

Figure 22: Large scale space-time evolution of the KSe in the full solution space with periodic boundary condition, 512 Fourier modes truncation, $L = 400\,, \nu = 1$.

chaos regime, the modes in the complement (infinite-dimensinal) space provide perturbations which drag solutions out of those subspaces and make them chaotic. If the resulting solutions are still close to the subspaces, they will bear many structural resemblance to the originally stable patterns with chaoticity caused by the weak interaction between them. The whole pattern forms out of instabilities of different levels and the chaotic dynamics just exhibits their competition and mutual saturation. In the periodic orbit theory, the most important recurrent patterns are captured by the shortest UPOs in both space and time, which encode the coarsest structure of the SIS in the phase space and contain the most unstable directions in their unstable manifolds. Longer cycles resolve more detailed structures and thus more subtle instabilities. The modest first step is to study the dynamics of systems with small sizes. It turns out that even these small systems have nontrivial dynamics and require much serious work. This direction was initially pursued by Christiansen *et. al* [37]. Using Newton-Raphson method, they located several hundred UPOs in the anti-symmetric space of the KSe with periodic boudary condition at the onset of spatiotemporal chaos, and accordingly established symbolic dynamics. The structure of the SIS was clearly displayed and physical averages were computed via trace formula in their pioneer work.

6.2 Dynamics of KSe at $L = 38.5\,, \nu = 1$

6.2.1 Qualitative dynamics and Fourier modes

It is always wise to develop a qualitative picture of the system dynamics before attempting an indepth investigation. Our preliminary results show that as the system size L increased, more and more stationary solutions appear, and that the chaotic attractor grows bigger and more complicated. 2-tori are generated through Hopf bifurcation of periodic orbits but higher-dimensional tori seem unlikely to occur, which is consistent with the claim made by Ruelle and Takens [219]. The local unstable manifolds of shortest periodic orbits found so far rarely achieve a dimension higher than two but the eigenvalues become bigger and bigger

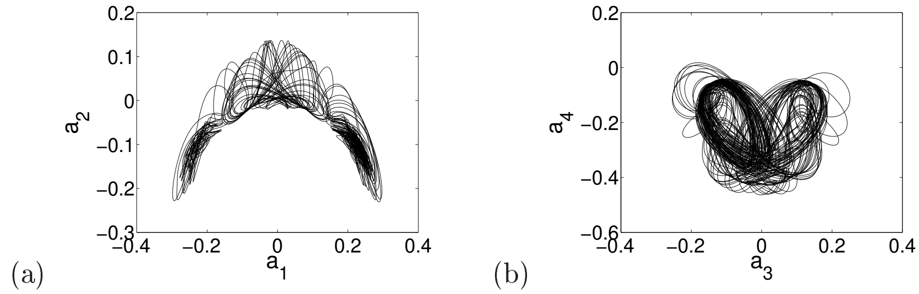

Figure 23: (a) a_1, a_2 projection of a typical phase orbit of (135); (b) a_3, a_4 projection of the same orbit; $L = 38.5\,, \nu = 1\,,$ 16 Fourier modes truncation.

in magnitude so that the Lyapunov dimension increases continuously. This is consistent with the linear growth of the fractal dimension of the SIS with the system size [247]. There might exist UPOs with many unstable directions [283], but they do not participate in the asymptotic dynamics at this stage.

For simplicity, We focus our attention also on the antisymmetric solution space of the KSe with periodic boundary condition. Christiansen *et al* investigated the chaotic dynamics at $L = 2\pi\,, \nu = 0.029910$ and 0.029924 or equivalently $\nu = 1\,, L = 36.31$ or $L = 36.30$, where the dynamics is a coarse periodic one [236] like that of the Rössler system [213]. We take $\nu = 1\,, L = 38.5$, where the KSe has qualitatively different dynamics.

How many Fourier modes are enough for our investigation. The optimal choice is using the least number of them to capture the interesting dynamics to the precision we want. For numerical computation, this is actually all we can do, since what we observe on the computer is always some coarsened version of the true dynamics. From a mathematical point of view, we often have relatively small number of active modes, and the rest are either slaved to the active ones or can be treated as negligible noises. The structural stability of short UPOs will guarantee the faithfulness of our numerical calculation. It is found that 16 modes are sufficient for our purpose [140, 125]. The results change very little (within a few percent) when we double the number of modes used. In particular, the chaotic dynamics and the UPOs are well preserved under this change.

6.2.2 Steady solutions and the dynamics

The SIS consists of three parts: the left part (S_L), the middle part (S_C) and the right part (S_R), see figure 23(a). S_L and S_R are related through the inversion symmetry mentioned previously, so only one of them needs to be considered, say, S_R. Each part has its own chaotic dynamics defined on a compact set and they communicate with each other occasionally. We will display part of the SIS on chosen Poincaré sections, build intrinsic coordinates along some unstable manifolds, draw the return map and search UPOs based on the return map. It turns out that this program is quite successful for S_C and needs further work for S_R.

A typical state on the SIS turns out to bear quite close resemblance to the steady solutions of (135). In figure 24, figure 25 and figure 26, the $u\,, u_x$ representations and the spatial profiles of three points on the SIS are shown in analogy to those of the steady

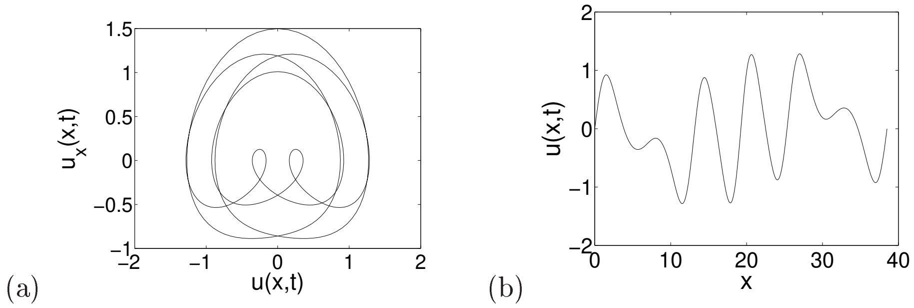

Figure 24: The spatial structure of $u(x,t)$ at a point on S_R, $L = 38.5\,, \nu = 1$, 16 Fourier modes truncation: (a) $u\,, u_x$ representation of the state; (b) Spatial profile of the same state.

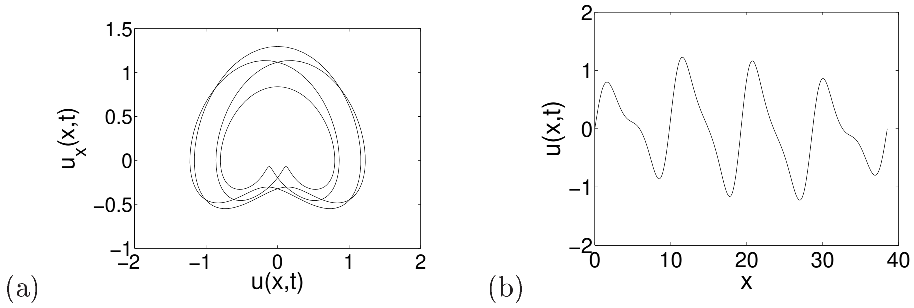

Figure 25: The spatial structure of $u(x,t)$ at a point on S_C, $L = 38.5\,, \nu = 1$, 16 Fourier modes truncation: (a) $u\,, u_x$ representation of the state; (b) Spatial profile of the same state.

solutions shown in the previous chapter. Note that figure 24 is similar to figure 19 and figure 25 is similar to figure 17. This correspondence, however, is not always possible. The state in figure 26 has no well defined steady counterpart. It is on the transition orbit from S_R to S_C and has 5 peaks. Remember that the steady state in figure 16 also has 5 peaks.

We also checked a lot of other states of the SIS and found that all of them have 4, 5 or 6 peaks and many of them are similar to the steady solutions. This means that the asymptotic dynamics take place in the neighborhood of the steady solutions which define in a coarse way the amplitude and the spatial structure of the states on the SIS. A typical phase orbit is moving in the frame set up by these steady ones. In this sense, we say that the phase space is partitioned by the steady solutions at the coarsest level. We will investigate more detailed structure of the SIS and the dynamics on it below.

6.2.3 Poincaré sections and intrinsic coordinates

After we felt comfort in the Gälerkin truncation of Fourier modes and developed a qualitative picture of the high-dimensional flow, we applied our variational method and succeeded in locating quite a few short UPOs. We initialized the search by checking the near recurrent orbit segments. We display here three shortest UPOs, named $p_C\,, p_{R1}\,, p_{R2}$, residing respectively in S_C (see figure 27), and in S_R (see figure 28, figure 29). Of course, each of them has a partner related by the inversion symmetry. All of them have only one unstable eigendirection. To conveniently visualize the unstable manifolds, the hypersurface $a_1 = 0$ is

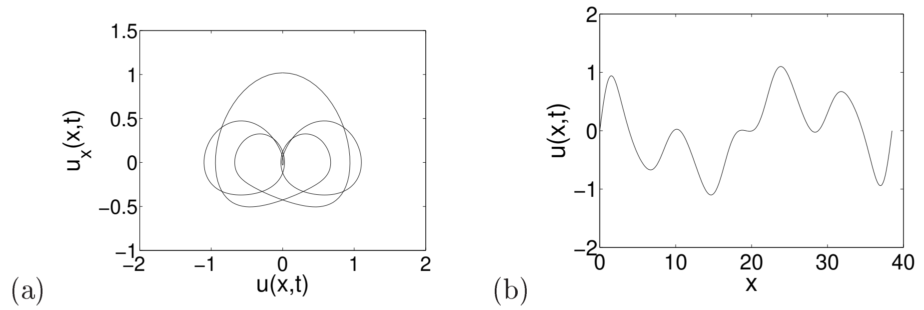

Figure 26: The spatial structure of $u(x,t)$ at a point on the transition line from S_R to S_C, $L = 38.5\,, \nu = 1\,,$ 16 Fourier modes truncation: (a) $u\,, u_x$ representation of the state; (b) Spatial profile of the same state.

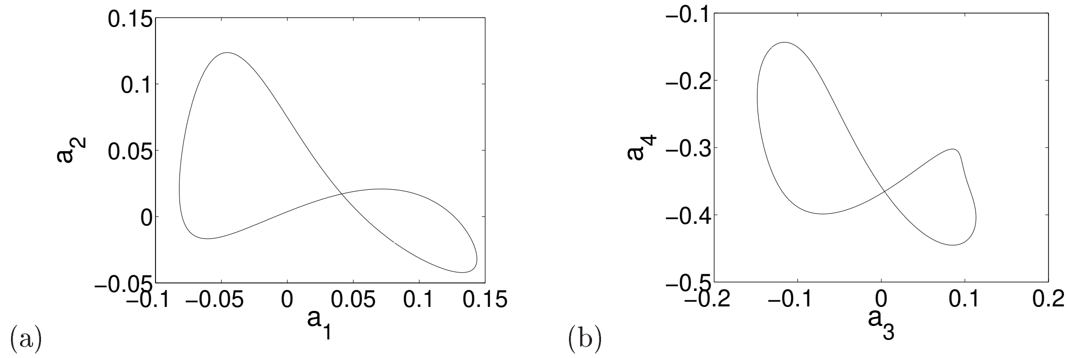

Figure 27: The shortest periodic orbit p_C in S_C, $T = 25.6356\,, L = 38.5\,, \nu = 1\,.$ (a) $a_1\,, a_2$ Fourier modes projection of the orbit; (b) $a_3\,, a_4$ projection of the same orbit.

chosen to be the Poincaré section in S_C. It contains the important 4-hump steady solution and seems to intersect transversally all the orbits in S_C. The period of p_C is $T = 25.6356$ and its largest three eigenvalues are $-6.6028\,, 1.0000\,, 0.0047$. Only one eigenvalue has magnitude bigger than one so the unstable manifold of p_C is one dimensional on the Poincaré section. We numerically continued the manifold from the eigenvector and displayed it in figure 30(a). Apparently, this is only part of the true manifold which has a fractal structure. We will use this part of the unstable manifold as the reference line L_C and assign a coordinate s to each point on it, where s is the length of the manifold between the point and the intersection of p_C with L_C. We use a minus sign to distinguish the two parts of L_C emanating from p_C.

To determine the coordinate of a point p_0 not on L_C, a point p_1 on L_C is located which is the closest to p_0 and $s(p_1)$ is assigned as the coordinate of p_0. In this way, an intrinsic coordinate system is built along the unstable manifold of p_C on the Poincaré section.

figure 30(b) shows the image of L_C after one iteration of the Poincaré map. While some of the points are mapped out of S_C, the image is visibly more complicated than than L_C itself. But still, the image is quite close to L_C and are well described by the intrinsic coordinate defined by L_C.

For S_R, the periodic orbit in figure 28 has a period $T = 20.0229$ with the largest three eigenvalues being $-1.7334\,, 1.0000\,, -0.43297$, and the one in figure 29 has a period

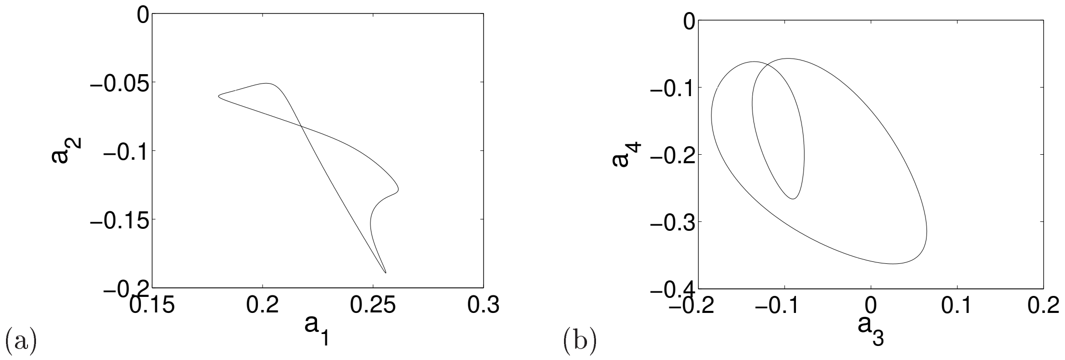

Figure 28: The first shortest periodic orbit p_{R1} in S_R, $T = 20.0229\,, L = 38.5\,, \nu = 1\,.$ (a) $a_1\,, a_2$ Fourier modes projection of the orbit; (b) $a_3\,, a_4$ projection of the same orbit.

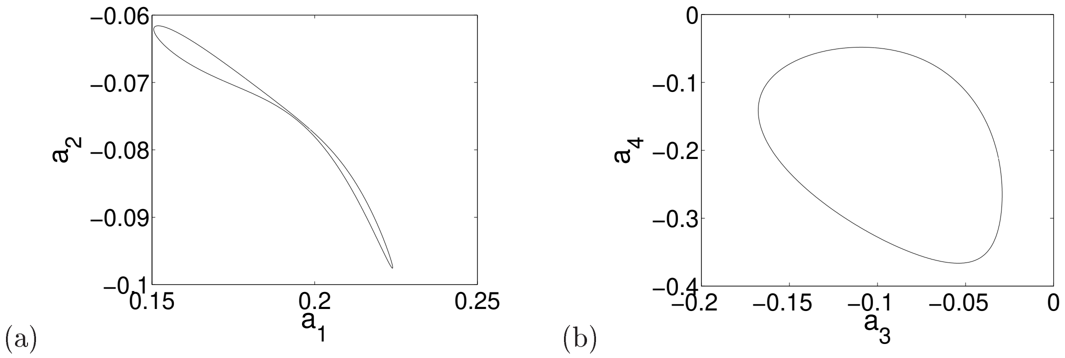

Figure 29: The second shortest periodic orbit p_{R2} in S_R, $T = 12.0798\,, L = 38.5\,, \nu = 1\,.$ (a) $a_1\,, a_2$ Fourier modes projection of the orbit; (b) $a_3\,, a_4$ projection of the same orbit.

$T = 12.0798$ with three leading eigenvalues being $-4.9839\,, 1.0000\,, 0.5633$. In all the three shortest cycles, the second largest eigenvalue is 1.0000, which corresponds to the eigendirection along the cycle and can be used as an indicator of accuracy of the numerical calculation. In our case, it is accurate up to 10^{-5}. We carry out the same program to p_{R2}. The Poincaré section is now defined by $a_4 = -0.122$, which is evidenced by figure 23. The reference unstable manifold L_R is shown in figure 31(a) and figure 31(b) displays the image of L_R after one iteration on the Poincaré section. We see that many new features appear in the image and thus L_R is not able to provide a good coordinate frame to describe S_R.

6.2.4 Return maps and periodic orbits

With the intrinsic coordinate, a simplified model of the dynamics on the SIS can be established. Its validity depends on how well the coordinate describes the SIS. We used the reference lines L_C and L_R and their one iteration images to construct the return map. The results are shown in figure 32. The chaos generating mechanism - stretching and folding are clearly seen in the diagram. The holes on the tips indicates communications between S_C and S_R or S_L.

Shown in figure 32(a) is a multi-modal map. We need at least 11 symbols to build the symbolic dynamics, each representing a monotone interval in the return map. The

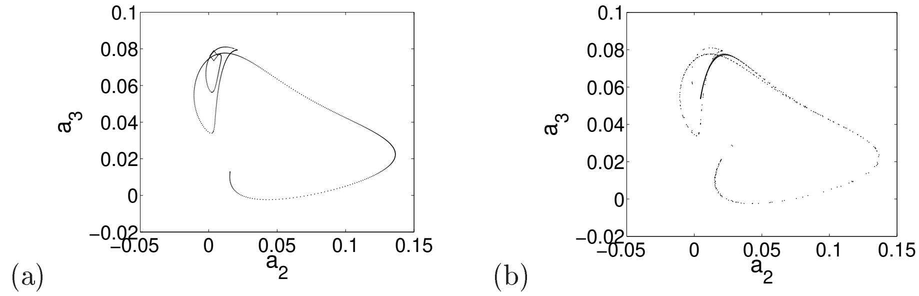

Figure 30: The unstable manifold of p_C and its first iteration on the Poincaré section $a_1 = 0$. (a) $a_2\,, a_3$ projection of the unstable manifold on the Poincaré section; (b) One Poincaré iteration of the unstable manifold projected to $a_2\,, a_3$ components.

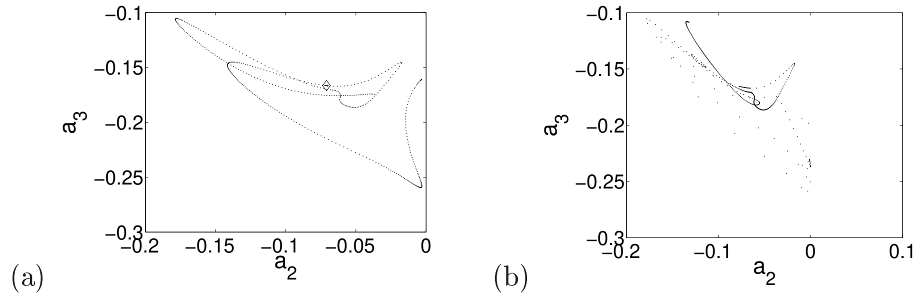

Figure 31: The unstable manifold of p_{R2} and its first iteration on the Poincaré section $a_4 = -0.122$. (a) $a_2\,, a_3$ projection of the unstable manifold on the Poincaré section; (b) One Poincaré iteration of the unstable manifold projected to $a_2\,, a_3$ components.

true dynamics can then be approximated by a subshift of finite type in the symbol space expanded by these symbols [51]. Note that the distribution of the points on the graph are highly non-uniform. This is due to the wide range of angles at which the orbits intersect the Poincaré section. The problem is even more serious for the return map of S_R as shown in figure 32(b) where points accumulate in the contracting parts and disperse at the stretching parts. So, the $1-d$ map established for S_R is not a good model of the true dynamics. Further investigation is needed.

From the return map, we may search the UPOs in a systematic way. To find all the UPOs of period n on the S_C Poincaré map, we may check the image of each point on L_C under nth iteration of the map. If the image has the same symbols with the starting point itself, then we can use the orbits generated by the point to initialize the search of a UPO of topological length n. We believe that in this way we can find all the short periodic orbits up to some given length if the $1-d$ model map is a good description of the original map on the Poincaré section.

By applying this searching technique, as a demonstration, we found more than one hundred UPOs on S_C. On S_R we are not so lucky, we found much less UPOs. On one hand, it is expected as there is much less stretchings and foldings in figure 32(b). On the other hand, the untrusted model map represented by figure 32(b) may give bad initializations which fail the searching program. An attracting cycle of period $T = 40.0565$ is shown in figure 33 which resides near S_R. Its basin of attraction is small as we never get to stay on it in the numerical simulation. A similar UPO of period $T = 60.1112$ is shown in figure 34.

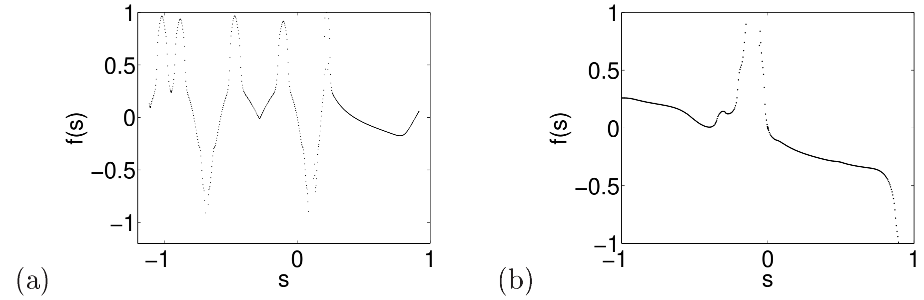

Figure 32: The return maps on the Poincaré sections using the intrinsic coordinates. (a) The return map for p_C on $a_1 = 0$; (b) The return map for p_{R2} on $a_4 = -0.122$.

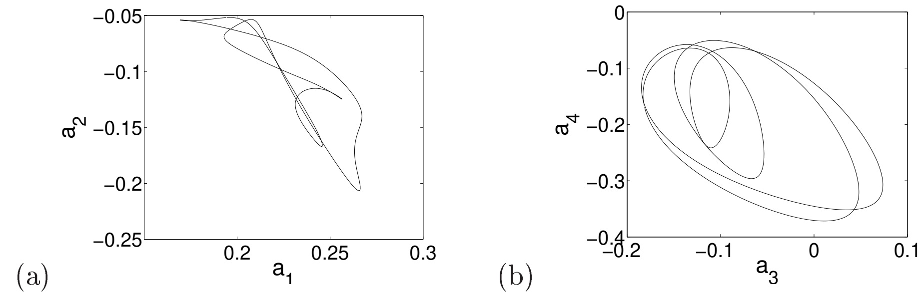

Figure 33: An attracting cycle of the KSe near S_R with the period $T = 40.0565$ in the antisymmetric solution space with periodic boundary condition; $L = 38.5$ and $\nu = 1$. (a) $a_1\,, a_2$ Fourier modes projection of the UPO; (b) $a_3\,, a_4$ Fourier modes projection of the UPO.

For S_R, a non-symmetric UPO of period $T = 81.3345$ is shown in figure 35 and a symmetric one of period $T = 77.4483$ is shown in figure 36.

6.3 Summary

In this chapter, we presented some preliminary results on the spatiotemporal dynamics of the KSe. The chaotic dynamics is generated through sequence of bifurcations and the coherent structures born in the bifurcations play an important role in later dynamics with bigger system size. We used the UPOs as a probe to explore the structure of the SIS and chaotic dynamics on it. Specifically, we investigated the dynamics of the KSe in the antisymmetric solution space with periodic boundary conditions at $L = 38.5\,, \nu = 1$. We built the intrinsic coordinates on the Poincaré section and plotted the return map. Many periodic orbits are found according to the return map. We found that if the return map is a good model of the true dynamics, then the initialization based on it is very effective; otherwise, bad.

There are lots of problems that need further investigation. First, how to choose a good Poincaré section is essential to the success of all subsequent steps. It should cut all the branches of the SIS transversely and should be numerically accessible. In the examples we discussed, we always choose some hyperplane. This is by no means the best. We did it only for numerical convenience. The more general Poincaré section should be a curved manifold. Second, even when the Poincaré section is well chosen, still much work has to be done to

Kuramoto-Sivashinsky system—)

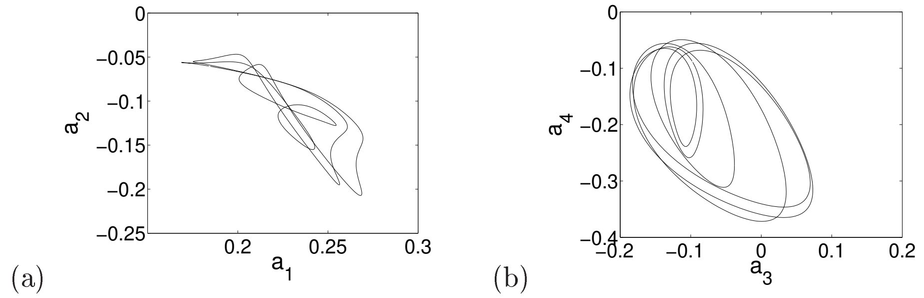

Figure 34: A UPO of the KSe on S_R with the period $T = 60.1112$ in the antisymmetric solution space with periodic boundary condition; $L = 38.5$ and $\nu = 1$. (a) a_1 , a_2 Fourier modes projection of the UPO; (b) a_3 , a_4 Fourier modes projection of the UPO.

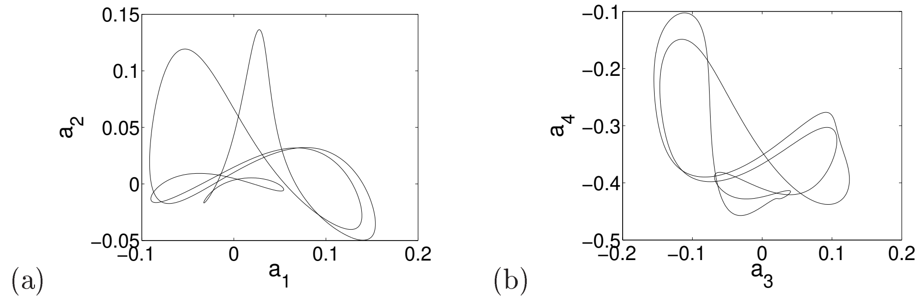

Figure 35: A non-symmetric UPO of the KSe on S_C with the period $T = 81.3345$ in the antisymmetric solution space with periodic boundary condition; $L = 38.5$ and $\nu = 1$. (a) a_1 , a_2 Fourier modes projection of the UPO; (b) a_3 , a_4 Fourier modes projection of the UPO.

determine the symbolic dynamics on the return map. Even when the unstable manifold of the shortest orbit is one dimensional, we may still need to consider their layout in the phase space. Like in the Hénon map, the symbolic regions may not be well partitioned by discrete points but by lines or other geometrical objects of even higher dimensions. Third, in order to capture the dynamics efficiently, other invariant objects like homoclinic or heteroclinic connections should be considered and used in the analysis.

A quite distinct approach is to discard the Poincaré section entirely and establish the symbolic dynamics directly in the phase space, since simple Poincaré sections may not be possible in general systems and our variational searching technique does not require one. How to identify regions of different dynamics and effectively partition the high-dimensional phase space is the biggest challenge we have to face. Some interesting work has been done for Hamiltonian systems [171, 32, 228] and may be generalized to the current case. The topological analysis carried out by Mischaikow *et al* [282, 184] provides clues how to do the partition in a systematic way in the general case.

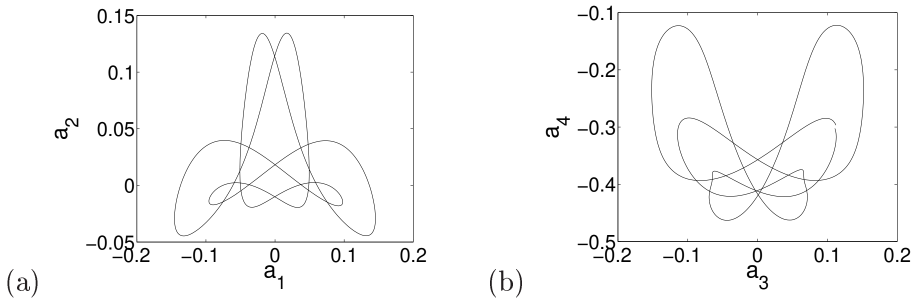

Figure 36: A symmetric UPO of the KSe on S_R with the period $T = 77.4483$ in the antisymmetric solution space with periodic boundary condition; $L = 38.5$ and $\nu = 1$. (a) $a_1\,, a_2$ Fourier modes projection of the UPO; (b) $a_3\,, a_4$ Fourier modes projection of the UPO.